# Air-sea heat flux control on the Yellow Sea Cold Water Mass intensity and implications for its prediction

Junying Zhu[a,b], Jie Shi[a,b,*], Xinyu Guo[a,c], Huiwang Gao[a,b], Xiaohong Yao[a,b]

[a] Key laboratory of Marine Environment and Ecology, Ocean University of China, Ministry of Education, 238 Songling Road, Qingdao 266100, China
[b] Laboratory for Marine Ecology and Environmental Sciences, Qingdao National Laboratory for Marine Science and Technology, Qingdao 266071, China
[c] Center for Marine Environmental Studies, Ehime University, 2-5 Bunkyo-Cho, Matsuyama 790-8577, Japan

## ARTICLE INFO

## ABSTRACT

The Yellow Sea Cold Water Mass (YSCWM), which occurs during summer in the central Yellow Sea, plays an important role in the hydrodynamic field, nutrient cycle and biological species. Based on water temperature observations during the summer from 1978 to 1998 in the western Yellow Sea, five specific YSCWM years were identified, including two strong years (1984 and 1985), two weak years (1989 and 1995) and one normal year (1992). Using a three-dimensional hydrodynamic model, the YSCWM formation processes in these five years were simulated and compared with observations. In general, the YSCWM began forming in spring, matured in summer and gradually disappeared in autumn of every year. The 8 °C isotherm was used to indicate the YSCWM boundary. The modelled YSCWM areas in the two strong years were approximately two times larger than those in the two weak years. Based on the simulations in the weak year of 1995, ten numerical experiments were performed to quantify the key factors influencing the YSCWM intensity by changing the initial water condition in the previous autumn, air-sea heat flux, wind, evaporation, precipitation and sea level pressure to those in the strong year of 1984, respectively. The results showed that the air-sea heat flux was the dominant factor influencing the YSCWM intensity, which contributed about 80% of the differences of the YSCWM average water temperature at a depth of 50 m. In addition, the air-sea heat flux in the previous winter had a determining effect, contributing more than 50% of the differences between the strong and weak YSCWM years. Finally, a simple formula for predicting the YSCWM intensity was established by using the key influencing factors, i.e., the sea surface temperature before the cooling season and the air-sea heat flux during the cooling season from the previous December to the current February. With this formula, instead of a complicated numerical model, we were able to roughly predict the YSCWM intensity for the following summer by using the data available online in winter.

## 1. Introduction

Cold water masses, also known as "cold pools", have been widely observed in shelf seas (Hill, 1996; Wyllie-Echeverria and Wooster, 1998; Brown et al., 1999; Horsburgh et al., 2000). They feature lower temperatures compared to their surrounding waters. However, the formation mechanisms of these cold water masses are not exactly the same. Many cold water masses are formed locally. Cold waters from the previous winter are locally trapped in a topographic depression after the onset of seasonal stratification, for example, the cold water masses in the Irish Sea (Hill et al., 1994), Middle Atlantic Bight (Houghton et al., 1982), North Sea (Warrach, 1998; Luyten et al., 2003), Yellow Sea (YS) (He et al., 1959; Hur et al., 1999; Wei et al., 2010; Yuan et al., 2013) and Bering Sea (Azumaya and Ohtani, 1995). Other cold water masses occur due to cold water intrusion from adjacent seas. For example, the Korea Strait Bottom Cold Water (KSBCW) is formed by the intrusion of near-bottom cold water from the Japan/East Sea (Johnson and Teague, 2002; Kim et al., 2006).

There are strong temperature gradients between cold water masses and surrounding waters, which generate special hydrodynamic processes, such as cyclonic circulation above the cold water mass (Hill, 1996; Horsburgh et al., 2000; Yu et al., 2016). Additionally, cold water masses play important roles in the distribution of nutrients and biological species. Brown et al. (1999) suggested that several species of fish and shellfish of commercial value (e.g., herring, plaice, turbot and *Nephrops norvegicus*) spawn in the North Sea cold pool. The cold water mass in the western Irish Sea generated a gyre that provided a physical retention of the planktonic larvae of Norway lobster and pelagic

---

juvenile fish (Dickey-Collas et al., 1997). Arctic species (e.g., Arctic cod) prefer to live in the cold water mass of the Bering Sea (Wyllie-Echeverria and Wooster, 1998). Therefore, intensity variations of cold water masses have significant impacts on the marine ecosystem (Dickey-Collas et al., 1997; Wyllie-Echeverria and Wooster, 1998; Stabeno et al., 2007; Na et al., 2010). The cold pool warming trend in the Bering Sea from 1988 to 2005 led to an ecosystem reorganization that favored pelagic over benthic predators (Grebmeier et al., 2006).

The YS is a semi-closed marginal sea in the northwest Pacific Ocean. A cold water mass called the Yellow Sea Cold Water Mass (YSCWM) occurs in the bottom layers in the central part of the YS (Hur et al., 1999; Zhang et al., 2008; Wang et al., 2014a, 2014b). It occupies ~30% of the total water volume in the YS during summer (Su and Weng, 1994). The YSCWM is also regarded as a nutrient-rich pool that contributes to the subsurface chlorophyll maximum phenomenon during summer and therefore affects primary production (Li et al., 2006; Wang et al., 2014a, 2014b; Liu et al., 2015; Xin et al., 2015). The key species of zooplankton (*Calanus sinicus*) is favored to survive the hot summer in the YSCWM (Wang et al., 2003). Consequently, the demersal fish stocks are closely related to the YSCWM intensity (Cho, 1982; Du et al., 1996).

The YSCWM intensity changes annually (Weng et al., 1989; Jiang et al., 2007; Park et al., 2011; Li et al., 2015, 2016a). The influencing factors reported by previous studies always fall into two aspects: remote factors and local atmospheric forcings. Park et al. (2011) suggested that the eastern YSCWM intensity is negatively correlated to the sea surface temperature and surface air temperature in the tropical to subtropical northwest Pacific Ocean by analyzing the data during 1967–2008 from the Korea Oceanographic Data Center (KODC) dataset. The intensity of the entire YSCWM simulated by Song et al. (2009) has a variation period of 5-years, which can be attributed to the El Niño-Southern Oscillation (ENSO) event. The Kuroshio Meander always induces a warmer YSCWM in the following year (Li, 1991; Jiang et al., 2007). Through statistical analyses, the YSCWM intensity is also associated with other climatic events, such as Arctic Oscillation (AO), Pacific Decadal Oscillation (PDO) and so on (Park et al., 2011; Li et al., 2015). These studies always focus on the response of the regional sea to climate change via teleconnection. However, it is difficult to explain the influencing mechanisms of remote factors on the YSCWM in detail.

Compared to remote factors, local forcing conditions have more direct effects on the YSCWM intensity. Several local atmospheric forcings related to the YSCWM intensity have been examined using correlation analyses. Based on the China Coastal Waters and Adjacent Seas Reanalysis (CORA) data from 1958 to 2008, Li et al. (2015) demonstrated that the local heat flux and wind stress in winter affected the YSCWM intensity (Song et al., 2009), while the local heat flux and wind stress in summer had a little impact. Jiang et al. (2007) found that the intensity of the northern YSCWM was primarily influenced by the air temperature in winter. Yang et al. (2014) stated that the lower the sea surface temperature was in February, the further south the boundary of the YSCWM was located. Additionally, the intensified thermocline from June to August blocks downward heat transport and then causes a cold event in the YSCWM (Park et al., 2011). Previous studies suggest that many important local factors determine the YSCWM intensity, but the contributions of each factor have not been estimated quantitatively.

Since the YSCWM intensity has a close relationship with the nutrient concentrations, primary production, and aggregation and migration of fish, it would be helpful to know the YSCWM intensity for the approaching summer in advance. Although some complicated numerical models can be used to achieve this goal, a simple and effective formula for prediction would be more convenient for those who are not familiar with models.

In this study, variations of the YSCWM intensity were examined and representative years of strong and weak YSCWM were identified based on observations from 1978 to 1999. In these representative years, a three-dimensional hydrodynamic model was used to reproduce the formation process of the YSCWM. Subsequently, a set of numerical
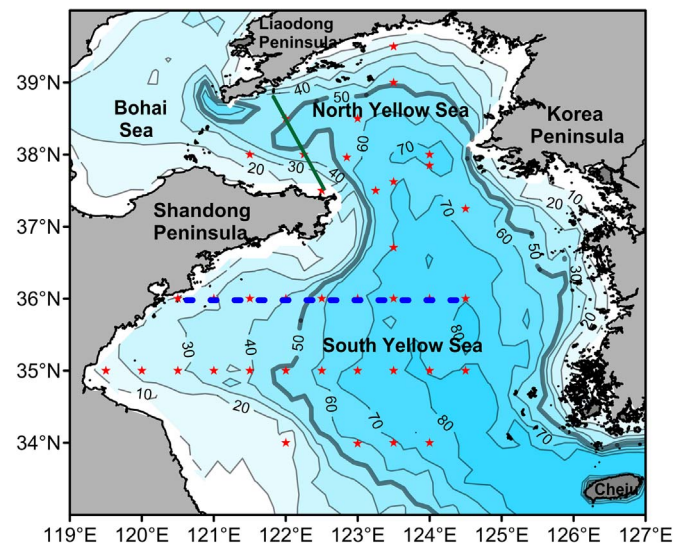


**Fig. 1.** Map of the Yellow Sea with topography. Grey solid contours denote bathymetry (in m), and the 50 m contour is bold. The observation stations are represented by red stars. The 36°N section is marked by a blue dashed line. The green solid line is the section from Dalian to Chengshan Jiao. (For interpretation of the references to color in this figure legend, the reader is referred to the web version of this article.)

experiments was performed to estimate the contributions of several local factors to the YSCWM intensity. Finally, a simple formula was proposed to predict the YSCWM intensity based on analyses of the influencing mechanism.

## 2. Materials and methods

### 2.1. Observation data

The observational water temperatures at standard depths (0, 10, 20, 30 and 50 m) in the YS (Fig. 1) in February and August from 1978 to 1998 were obtained from the archives at the State Oceanic Administration (SOA) of China. The observed area covered the western area of the YS. Over the entire analysis period (1978–1998), there were no data for February for the years 1984, 1996, 1997, and August 1993 (Table 1). Following the previous studies (Guan, 1963; Li, 1991; Li et al., 2015), we used an isotherm of 8 °C as the boundary of the YSCWM.

The YSCWM can be easily identified from the horizontal distribution of water temperatures observed at a depth of 50 m (Fig. 2a) and the vertical distribution of temperatures along the 36°N section (Fig. 2b). The YSCWM was isolated from ambient warmer waters by strong temperature fronts (Fig. 2a) and thermoclines (Fig. 2b).

To quantify the YSCWM intensity during summer, we defined four indices, namely, the average water temperature inside the YSCWM and the YSCWM area at a depth of 50 m as well as those along the 36°N section in August. The observation stations in August were primarily located in the western region of the YS, with slight differences in each year. To maintain a consistent observation area throughout the entire analysis period, we defined a fixed area from 35°N to 38°N and from 122.2°E to 124.0°E (the orange rectangle in Fig. 2a) and identified the YSCWM using the 8 °C isotherm in the area. Along the 36°N section, the observed area covered as far as 124.0°E in the east for most years

**Table 1**
The observation years.

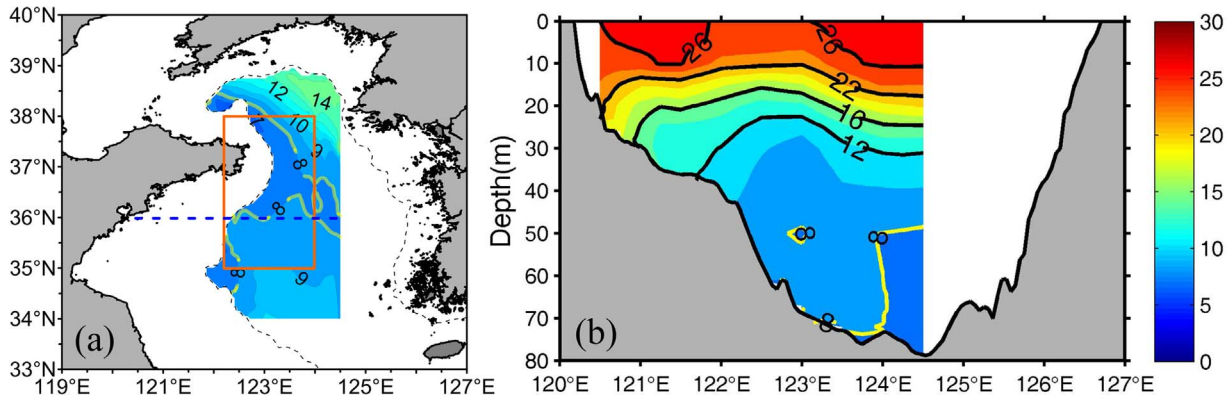| Month | Years with observation |
| --- | --- |
| February | 1978–1983, 1985–1995, 1998 |
| August | 1978–1992, 1994–1998 |

**Fig. 2.** The distribution of multi-year average water temperature (°C) in August from 1978 to 1998 at the depth of 50 m (a) and along the 36°N section (b). The orange rectangle is the calculating area from 35°N to 38°N and from 122.2°E to 124.0°E. (For interpretation of the references to color in this figure legend, the reader is referred to the web version of this article.)

except for 1995. Therefore, we set the eastern boundary of calculating area as 124.0°E and used a linear extrapolation to horizontally extend the observation area from 123.5°E to 124.0°E in 1995.

The YSCWM intensity was defined by comparing the anomaly of the four indices in each year with their mean ranges of changes over the entire analysis period (Zhang and He, 1981). $X$ was set to be any of the four indices, and $\overline{X}$ was the mean value of $X$ from 1978 to 1998. $\Delta X_i$ was anomaly of $X$ at the year of $i$:

$$\Delta X_i = X_i - \overline{X} \tag{1}$$

Its mean range of change over entire study period is denoted by mean value of the absolute value of $\Delta X_i$:

$$\overline{|\Delta X|} = \frac{1}{n} \sum_{i=1}^{n} |\Delta X_i| \tag{2}$$

where $n$ was total number of years. The comparison for the four indices were presented in Table 2, in which the symbol "-" was marked when the anomaly of an index in a year ($\Delta X_i$) was smaller than $-\frac{1}{2}\overline{|\Delta X|}$; "+" was marked when $\Delta X_i$ was larger than $\frac{1}{2}\overline{|\Delta X|}$; "O" was marked when $\Delta X_i$ was between $-\frac{1}{2}\overline{|\Delta X|}$ and $\frac{1}{2}\overline{|\Delta X|}$.

A strong YSCWM year was characterized by low temperatures and large areas both horizontally and vertically, while a weak YSCWM year by high water temperatures and small areas. If the two temperature

indices for one year were marked with a '-' and the two area indices were marked with a "+", we identified the year as a strong YSCWM year (Table 2). On the contrary, if the two indices for the water temperature were marked with a "+" and the two indices for the area with a "-" for a certain year, we defined the year to be a weak YSCWM year. If all four indices for one year had the symbol "O", it was a normal YSCWM year. For the years not marked as strong, weak, or normal years, we considered them to be atypical years for the YSCWM intensity.

## 2.2. Model description and configuration

The three-dimensional hydrodynamic model used in our study was based on the Princeton Ocean Model (Blumberg and Mellor, 1987; Mellor, 2003) and was configured with a nesting method to obtain a high horizontal resolution (1/18°) for the Kuroshio simulation (Guo et al., 2003). There were 21 sigma layers in the vertical direction. Based on Guo et al. (2003), Wang et al. (2008) used the same model for a smaller model domain covering the Bohai Sea, YS and East China Sea, but added the tidal forcing ($M_2$, $S_2$, $K_1$ and $O_1$ tides) along the lateral boundary and freshwater input from the sea surface and rivers.

Our model domain was 117.5–131.5°E and 24.0–41.0°N. The external and internal time steps were 6 s and 360 s, respectively. The model was driven by the monthly mean river runoff, monthly sea surface salinity, daily air-sea heat flux, daily wind stress, daily surface level pressure, daily precipitation and evaporation rates. The daily air-sea heat flux in the model ($Q_{net\_model}$) was the net sea surface heat flux from the NCEP reanalysis dataset ($Q_{net\_NCEP}$) plus an adjustment term proportional to the difference between the sea surface temperature from the NCEP reanalysis ($T_{NCEP}$) and simulated sea surface temperature ($T_{model}$) as follows:

$$Q_{net\_model} = Q_{net\_NCEP} + \frac{\partial Q}{\partial T}(T_{model} - T_{NCEP}) \tag{3}$$

where the coefficient $\frac{\partial Q}{\partial T}$ is $-50$ W/m² K$^{-1}$ (Ezer and Mellor, 1992). The $Q_{net\_NCEP}$ was the sum of shortwave radiation flux, longwave radiation flux, latent heat flux and sensible heat flux. The daily atmospheric forcing was determined by averaging the original 6 hourly products from the NCEP/DOE reanalysis (https://www.esrl.noaa.gov/psd/data/gridded/data.ncep.reanalysis.html). The initial conditions in January were from a nested ocean model with the same resolution (NEST3 in Guo et al., 2003) and monthly open boundary conditions were from a large domain model with a coarse resolution (NEST2 in Guo et al., 2003). The river runoffs were obtained from the Marine Atlas of the Bohai Sea, Yellow Sea, and East China Sea: Hydrology (Chen, 1992).

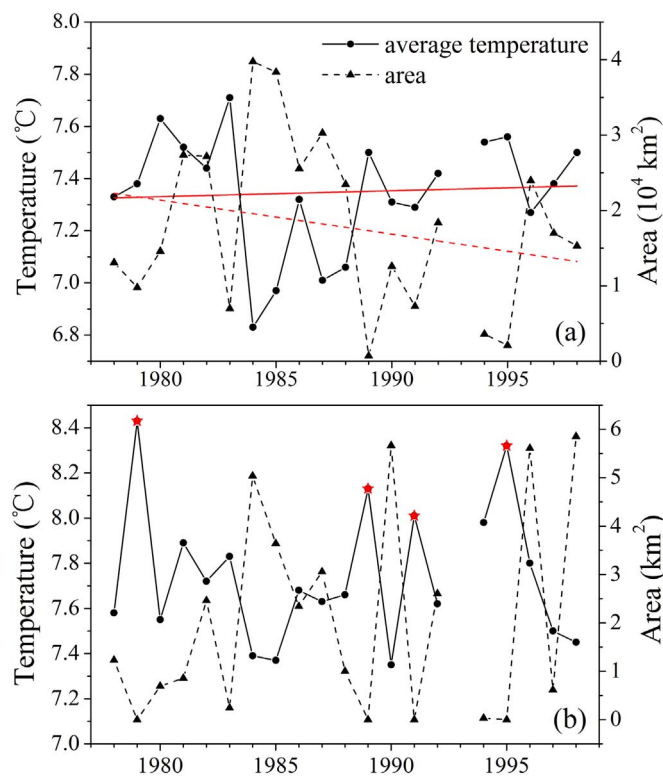Before simulating the formation process of the YSCWM in a specific

**Table 2**
The YSCWM intensity in August.

| Year | The 50 m depth | | The 36°N section | | Grade |
|------|---------------------|------|---------------------|------|--------|
|      | Average temperature | Area | Average temperature | Area |        |
| 1978 | O | O | - | O |        |
| 1979 | O | - | + | - |        |
| 1980 | + | O | - | - |        |
| 1981 | + | + | + | - |        |
| 1982 | + | + | O | O |        |
| 1983 | + | - | O | - |        |
| 1984 | - | + | - | + | strong |
| 1985 | - | + | - | + | strong |
| 1986 | O | + | O | O |        |
| 1987 | - | + | O | + |        |
| 1988 | - | + | O | - |        |
| 1989 | + | - | + | - | weak   |
| 1990 | O | - | - | + |        |
| 1991 | O | - | + | - |        |
| 1992 | O | O | O | O | normal |
| 1994 | + | - | O | - |        |
| 1995 | + | - | + | - | weak   |
| 1996 | O | + | + | + |        |
| 1997 | O | O | - | - |        |
| 1998 | + | O | O | + |        |

**Fig. 3.** Time series of the average water temperature (°C) and the YSCWM area (km²) at a depth of 50 m (a) and along the 36°N section (b) in August. The solid and dashed red lines in (a) are the linear trends of water temperature and area. The years when the YSCWM is not observed are marked with red stars in (b). (For interpretation of the references to color in this figure legend, the reader is referred to the web version of this article.)

year, we started the calculation in January with a climatological initial condition and adopted a spin-up mode by running the model for three years with the air-sea flux and other inputs from the year before the specified year. Then, the sea surface forcing was changed to those of the following specified year to simulate the water conditions of that year. The model results from September of the third year to August of the following specified year were used to examine the formation of the YSCWM.

## 3. Results

### 3.1. Definition of the YSCWM intensity using observation data

The YSCWM showed significant interannual variations in terms of the average water temperature and area (Fig. 3). At a depth of 50 m, the average water temperature inside the YSCWM varied from 6.83 °C (1984) to 7.71 °C (1983) from 1978 to 1998, with an average water temperature of 7.35 °C (Fig. 3a). A slightly increasing trend of 0.0023 °C/y was determined using a linear regression. The YSCWM area had its maximum value of $3.9 \times 10^4$ km² in 1984, which was almost 50 times the minimum value of 700 km² in 1989. The YSCWM area at a depth of 50 m had a multi-year average value of $1.8 \times 10^4$ km² and a declining trend at a rate of 452 km²/y from 1978 to 1998. The correlation coefficient between the average water temperature and the YSCWM area was − 0.73 (Fig. 3a).

Along the 36°N section, the average water temperature inside the YSCWM was the lowest in 1990 (7.35 °C) and highest in 1994 (7.98 °C) (solid line in Fig. 3b). The YSCWM area along the section changed from zero to 6 km² (dashed line in Fig. 3b). The zero area of the YSCWM appeared in 1979, 1989, 1991 and 1995 when there was no water with a temperature lower than 8.0 °C in August along this section in the

calculating area. Because of the absence of the YSCWM in these four years, we highlighted the lowest water temperature along the section in Fig. 3b with red stars. A significantly negative correlation (− 0.69) was shown between the average water temperature and the YSCWM area along the section (Fig. 3b).

The negative correlations between the water temperature and the YSCWM area at a depth of 50 m and along the 36°N section indicated a stronger YSCWM with a lower water temperature and larger area at the same time. In addition, the YSCWM variations in the horizontal and vertical directions were generally consistent with each other. The correlation coefficient between the average water temperatures of the YSCWM at a depth of 50 m and along the 36°N section was 0.48, and the correlation coefficient between the YSCWM areas was 0.56.

The four indices for the YSCWM intensity from 1978 to 1998, as defined in Section 2.1, were given in Table 2. The YSCWM experienced a colder (stronger) period from 1984 to 1988 and a warmer (weaker) period from 1989 to 1995. According to the consistency among the four indices shown in Table 2, 1992 was defined as a normal YSCWM year, 1984 and 1985 as strong YSCWM years, and 1989 and 1995 as weak YSCWM years. In the following sections, the controlling factors on the YSCWM intensity were investigated by comparing the simulated formation processes of the YSCWM in the strong years (1984 and 1985), weak years (1989 and 1995) and normal year (1992).

### 3.2. The formation process of the YSCWM

The model results in the normal year of 1992 were used to examine the formation process of the YSCWM. The modelled water temperatures were consistent with the observations in 1992 (Fig. 4d), with a correlation coefficient of 0.98 in February and 0.93 in August. Compared to the observations, 80% of the model results fell into the error range of 10% and 91% were within the error range of 20%. Since the modelled water temperatures were averaged monthly, while the observations were fixed-point measurements at a specific time, some discrepancies were expected. Comparing the modelled and observed horizontal and vertical distributions of water temperature, it was indicated that the model reasonably captured the major hydrological features in the YS (Fig. 5 and Fig. 6). Both model results and observations showed the horizontal domination of the Yellow Sea Warm Current in winter (Fig. 5b and Fig. 6b) and the YSCWM in summer (Fig. 5d and Fig. 6d), and vertically well mixing (Fig. 5f and Fig. 6f) in winter and strong stratification in summer (Fig. 5h and Fig. 6h). The thermocline began to form in spring (Fig. 5g and Fig. 6g) and gradually disappeared in autumn (Fig. 5e and Fig. 6e). Besides, observed multi-year average temperatures in August (Fig. 2) were similar with those in the normal of 1992 (Fig. 6d, h), which indicated the model capacity to reproduce the averaged YSCWM. Consequently, we used the model results (Fig. 5) to analyze the processes from disappearance of the YSCWM in last autumn to maturity of this YSCWM in current summer.

In autumn (November) of the previous year (1991), the stratification became weak with the increase of wind speed and decrease of solar radiation. Consequently, the YSCWM almost vanished (Fig. 5a, e). The area surrounded by the 8 °C isotherm shrunk to a very small area at a depth of 50 m. Along the 36°N section, water with a temperature less than 8 °C was found below the depth of 50 m and occurred only between 124°E and 125°E. In winter, the water temperature was vertically homogeneous (Fig. 5f) due to the strong vertical mixing caused by the strong winter monsoon and surface cooling. At a depth of 50 m, a northward warm tongue was found along the YS central trough (Fig. 5f) and the 8 °C isotherm extended northward to 35–36°N (Fig. 5b), indicating the presence of the Yellow Sea Warm Current. In spring, the water temperature in the upper layer rose (Fig. 5g) with the increase of solar radiation and decrease of wind speed since winter. The thermocline formed at a depth of ∼ 15 m. Cold water remained in the deep layer of the YS trough. The Yellow Sea Warm Current gradually weakened, and the YSCWM began to form (Fig. 5c, g). There were three low
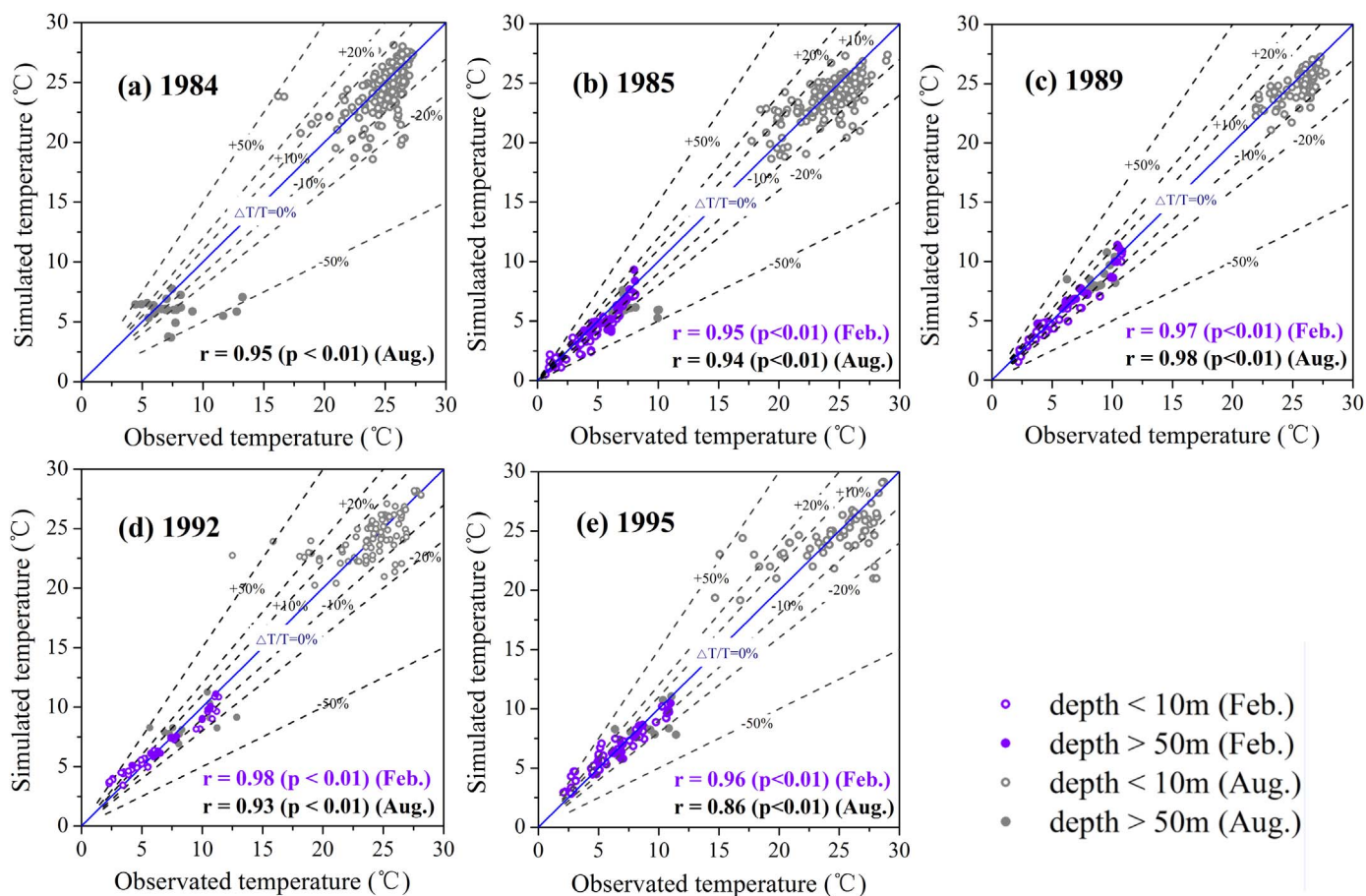
**Fig. 4.** The comparison between the simulated and observed water temperatures. The blue solid line denotes the 1:1 line. (For interpretation of the references to color in this figure legend, the reader is referred to the web version of this article.)

temperature cores at a depth of 50 m (Fig. 5c). One lied in the north YS, and the other two cores were located at the eastern and western part of the south YS. In summer, the sea surface temperature reached up to 26 °C, while the temperature of the deeper water was below 8 °C (Fig. 5h). The three cold cores at a depth of 50 m in spring merged to form the isolated YSCWM (Fig. 5d).

The simulated water temperature in other years showed similar seasonal variations compared to the normal year of 1992. In general, the YSCWM began forming in spring, matured in summer and gradually disappeared in autumn every year. Besides, the observations also indicated that the YSCWM intensity had significant interannual variations (Fig. 3).

### 3.3. Strong and weak years of the YSCWM

The years 1984 and 1985 were strong years for the YSCWM, while 1989 and 1995 were weak years for the YSCWM (Table 2). The model simulated these four years with the same procedures performed for the normal year of 1992. Fig. 4 showed the comparisons of the water temperatures between the model results and observations in February and August for these four years. The correlation coefficients between the simulations and observations were 0.95, 0.95, 0.98 and 0.86 in August of 1984, 1985, 1989 and 1995, respectively. On average, more than 90% of the simulated water temperatures fell into an error range of 20%. Although the modelled average temperature within the YSCWM was a little lower than the corresponding observed value in the same year, the model reproduced the lower temperature of the YSCWM in the strong years (1984 and 1985) and higher temperature of the YSCWM in the weak years (1989 and 1995) (Table 3). Consequently, we were able to use the model results to analyze the differences of the YSCWM in the

whole YS between strong and weak YSCWM years.

From modelled distribution of water temperature at a depth of 50 m (Fig. 7a-d), the YSCWM was located in the central trough of the YS. The northern boundary of the YSCWM reached approximately 39°N in both the strong years and weak years. However, the southern boundary of the YSCWM changed annually, from 33.5°N in the strong years of 1984 and 1985 to approximately 35°N in the weak years of 1989 and 1995. Consequently, the YSCWM areas at a depth of 50 m in the strong years ($1.15 \times 10^5$ km$^2$ in 1984 and $1.05 \times 10^5$ km$^2$ in 1985) were much larger than those in the weak years ($4.73 \times 10^4$ km$^2$ in 1989 and $4.31 \times 10^4$ km$^2$ in 1995).

Along the 36°N section (Fig. 7e-h), the deep cold water was isolated from the surface warm water by a strong thermocline with a temperature gradient of 2–3 °C/m. The YSCWM within the 8 °C isotherm usually had two cold cores, i.e., the eastern core and western core. In the strong years of 1984 and 1985, the two cold cores were relatively stable. The lowest water temperature of the western core was 3.44 °C, while that of the eastern core was 4.86 °C. In the weak years of 1989 and 1995, the eastern cold cores also occurred, and the lowest water temperatures were 7.21 °C and 7.20 °C in 1989 and 1995, respectively. However, the western cold core was not stable, i.e., it occurred in 1989, with the lowest water temperature of 7.57 °C, but did not occur in 1995.

The period from the previous autumn to the summer of a specific year was the formation period of the YSCWM. During this period, the average water temperature, both at the sea surface and a depth of 50 m, showed similar seasonal variations in all five years (Fig. 8a, b). However, the water temperatures at the sea surface and a depth of 50 m exhibited different variations. In the previous autumn (September), when the previous YSCWM began to disappear, the sea surface temperature decreased due to atmospheric cooling, while the temperature
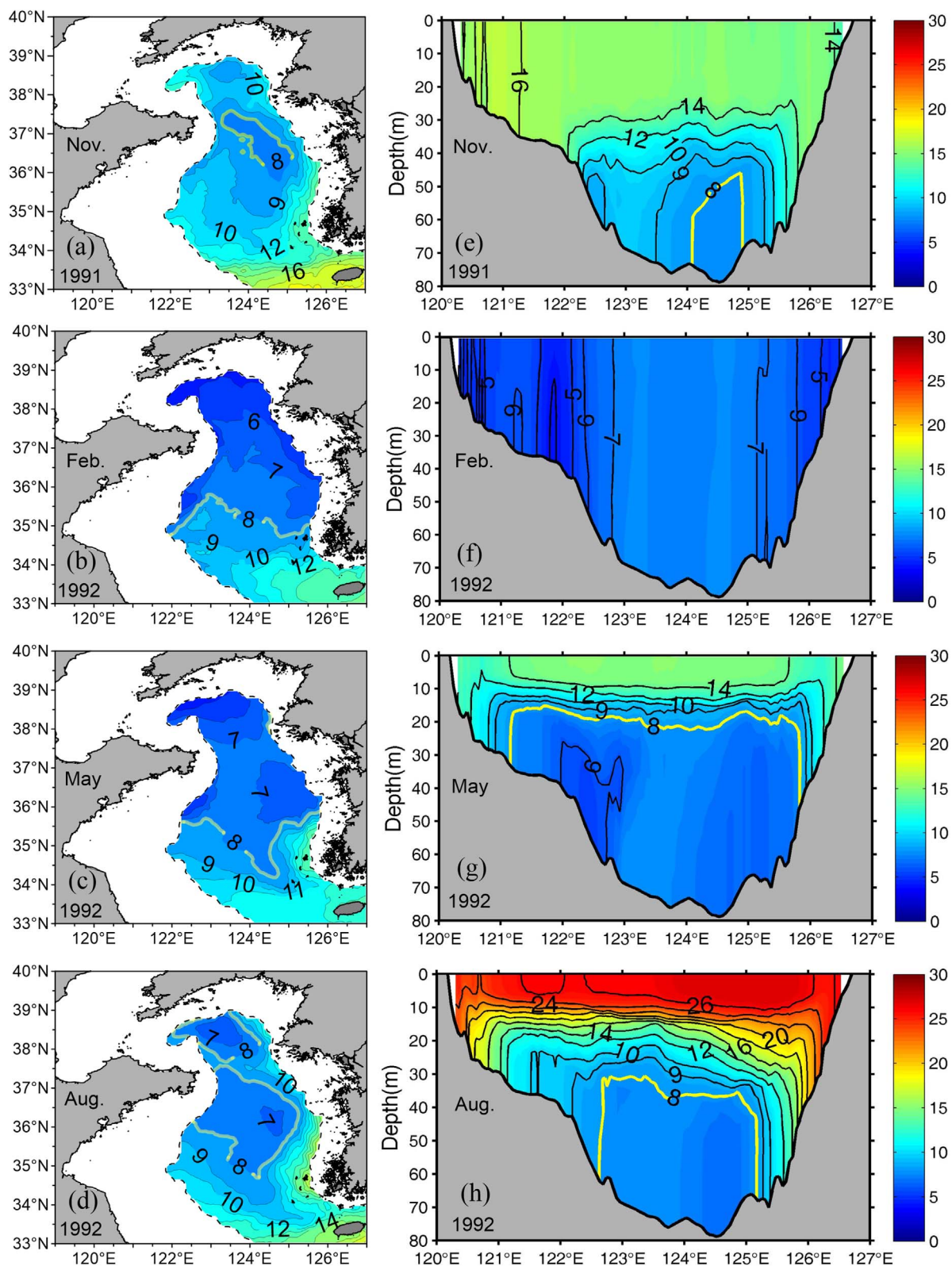
**Fig. 5.** The seasonal distribution of the simulated water temperatures (°C) in the normal year of 1992 at a depth of 50 m (a)–(d) and along the 36°N section (e)–(h). The dashed line denotes the 50 m isobath.

at a depth of 50 m increased since the thermocline was gradually broken and the heat flux was transported downward to the deep water layer. In the previous winter, the water temperature was vertically homogeneous and the water temperature of the entire water column decreased. Subsequently, in the following spring and summer, the water

temperature gradually increased both at the sea surface and at a depth of 50 m. The increasing rate was much faster at the sea surface than that at a depth of 50 m. A similar seasonal variation of the YSCWM was also observed at a station near the YSCWM boundary by Li et al. (2016b).

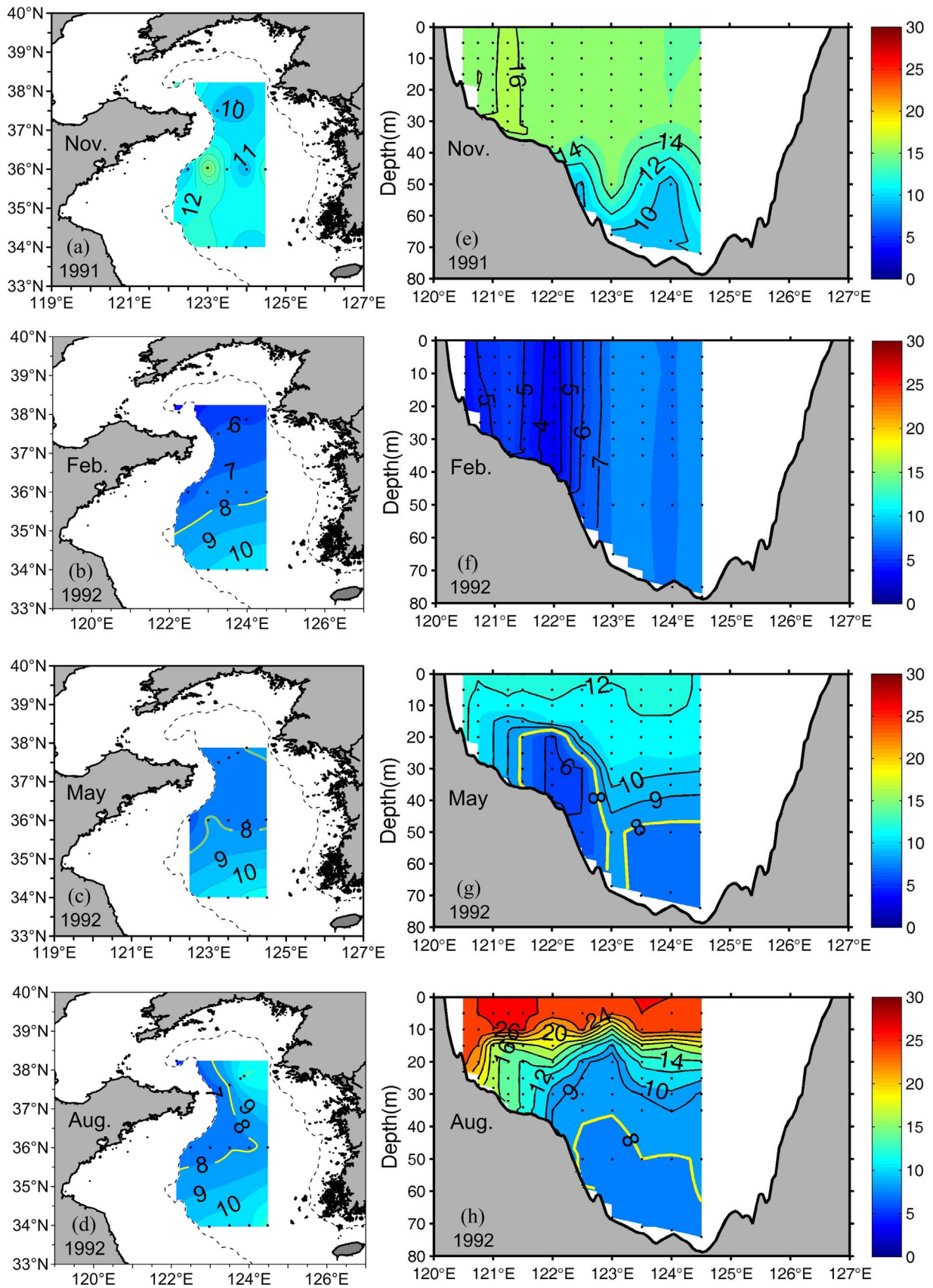Using the normal year of 1992 as a reference, the temperature

**Fig. 6.** As Fig. 5, but for observation. The black dots are observation stations.

**Table 3**
Comparison of the simulated and observed water temperatures (°C) for the YSCWM in August during the representative years of the YSCWM.

| Year | Average temperature at a depth of 50 m | | Average temperature along the 36°N section | |
|------|-------|-------------|-------|-------------|
|      | Model | Observation | Model | Observation |
| 1984 | 6.06  | 6.83        | 5.24  | 7.39        |
| 1985 | 6.19  | 6.97        | 6.10  | 7.37        |
| 1992 | 7.63  | 7.42        | 7.73  | 7.55        |
| 1989 | 7.71  | 7.50        | 7.85  | > 8.0       |
| 1995 | 7.67  | 7.56        | 7.84  | > 8.0       |

anomalies between the other four years and 1992 were determined at both the sea surface (Fig. 8c) and at a depth of 50 m (Fig. 8d). From the previous September to December, the water temperatures in the strong years of the YSCWM were not necessarily lower than those in the weak years either at the sea surface or at a depth of 50 m. The sea surface temperature in the strong years (1984 and 1985) almost always showed positive temperature anomalies, while the sea surface temperature in the weak years (1989 and 1995) showed positive and negative anomalies alternatively. At a depth of 50 m, the water temperatures in the strong year of 1984 and weak year of 1989 were similar to those in the normal year of 1992, as indicated by their small temperature anomalies. Therefore, the period from September to November was not the key time that determined the YSCWM intensity for the following summer.

During the cooling season from December to February, the variations of the water temperature anomalies at the sea surface were similar with those at a depth of 50 m (Fig. 8c, d). The water temperature had negative anomalies in the strong years of the YSCWM. Although the temperature anomalies were not always positive in the weak years, their values were much higher than those in the strong YSCWM years. From spring to summer, the variations of the water temperature anomalies at the sea surface and at a depth of 50 m were significantly different due to the strong stratification. At the sea surface, the differences of the water temperature anomalies among these five years were not as significant as those in winter. However, the water temperature anomalies at a depth of 50 m remained approximately the same as those in the previous cooling season. The water temperature anomalies in the strong years of 1984 and 1985 were almost 2 °C lower than those in the weak years of 1989 and 1995. In the deep layer of the central YS (Fig. 8d), the consistency of water temperature anomalies from the previous winter to the following summer indicated that the cooling process in the previous winter was critical for determining the YSCWM intensity in summer.

The area where water temperature was lower than 8 °C at a depth of 50 m decreased in the previous autumn, sharply increased in the previous winter and then slightly decreased in the following spring and summer during these five years (Fig. 9). In the previous autumn, the area was largest in the strong year of 1985 and smallest in the weak year of 1995. However, the area in the strong year of 1984 was approximately the same as that in the weak year of 1989, both of which were larger than that in the normal year of 1992. Subsequently, during the cooling season, the areas in all five years increased rapidly due to strong vertical mixing and enhanced heat loss at the sea surface. At the end of the cooling season, the areas in the two strong years were significantly larger than those in the two weak years, and the area in the normal year of 1992 was between the areas in the strong years and weak years, which was the case until the formation of the YSCWM in summer. In 1984 (the strongest year), the cold water area with temperatures less than 8 °C was larger than that in 1995 (the weakest year), $4.8 \times 10^4$ km² larger in February and $7.0 \times 10^4$ km² larger in August, showing that 69% of the difference was preserved from the previous winter to summer.

### 3.4. Key factors controlling the YSCWM intensity

To quantitatively investigate the effects of several factors on the YSCWM intensity, several numerical experiments were designed based on the reference years of 1984 (a strong YSCWM year) and 1995 (a weak YSCWM year), and the details of each simulation are listed in Table 4. The simulation of 1995 was set to be the control run. The forcing conditions, including the initial conditions, wind, evaporation, precipitation, sea level pressure and air-sea heat flux, were changed to those of 1984 in the experiments labelled as INITIAL, WIND, EVA, PRE, SLP and HEAT, respectively. In these experiments, except for the factors in Table 4, the other input data for model were the same as those in the simulation for 1995. To quantify the contributions of these factors to the differences between the two reference years (1984 and 1995) in terms of the water temperature and area of the YSCWM, the contribution rate ($\alpha$) was calculated using the following formula:

$$\alpha = \frac{M_{Exp} - M_{weak}}{M_{strong} - M_{weak}} \times 100\% \tag{4}$$

where $M_{Exp}$ is the average water temperature inside the YSCWM or the YSCWM area in August in each numerical experiment. $M_{strong}$ is the corresponding value in 1984, and $M_{weak}$ is the corresponding value in 1995. The contribution rates obtained from those sensitivity experiments were showed in Table 5.

The results of the experiments indicated that the air-sea heat flux was the dominant factor influencing the YSCWM intensity, which contributed about 80% and 74% to the differences of the average water temperature and the YSCWM area at a depth of 50 m, respectively, and 49% and 91% to those along the 36°N section, respectively. The secondary factor was the initial water conditions in the previous autumn when the previous YSCWM tended to fade, which contributed around 10% of the differences in the water temperature of the YSCWM in the following year. The influence of wind in the experiment WIND included hydrodynamic processes, such as mixing and convection. Wind had a negative influence (approximately − 6% to temperature at a depth of 50 m) on the YSCWM intensity. The average meridional wind speed in the previous winter of 1984 as well as for WIND was 4.9 m/s, which was larger than the value of 4.2 m/s in 1995. Under the stronger winter monsoon, the Yellow Sea Warm Current intruded more northward along the YS trough (Lie et al., 2001; Oh et al., 2013). Consequently, water with higher temperatures remained to form the warmer YSCWM. Additionally, other sea surface forcing, including evaporation, precipitation and sea level pressure, had only a little impact on the YSCWM intensity.

Since the air-sea heat flux plays the most important role in the YSCWM intensity, four additional numerical experiments were performed to know which season of the air-sea heat flux was the determining factor. The air-sea heat flux from the previous autumn (from previous September to November), previous winter (from previous December to this February), this spring (from March to May) and this summer (from June to August) were changed from 1995 to 1984 in the experiment Autumn-HEAT, Winter-HEAT, Spring-HEAT and Summer-HEAT, respectively. It was found that the air-sea heat flux in the previous winter was the primary factor, contributing 64% and 58%, respectively, of the differences of the average water temperature and area of the YSCWM at a depth of 50 m, while along the 36°N section, the contributions were 40% and 76%, respectively. The secondary factor was the air-sea heat flux in spring, followed by that in the previous autumn. The contribution of the summer air-sea heat flux to the difference of the YSCWM intensity in two years was nearly zero.

The results of the numerical experiments can also be interpreted based on the time series of the air-sea heat flux in different years (Fig. 10). The air-sea heat flux of different years varied more significantly in the previous winter than the other three seasons. The air-sea heat flux in the previous winters of 1984 and 1985 (the strong
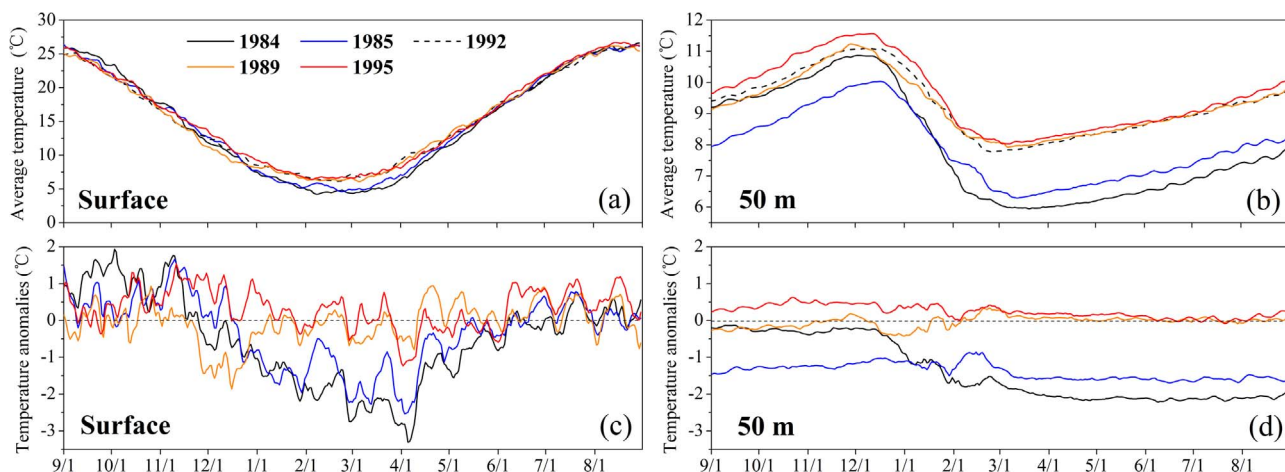
**Fig. 7.** The distribution of modelled water temperatures (°C) at a depth of 50 m (a)–(d) and along the 36°N section (e)–(h) in two strong YSCWM years (1984,1985) and weak YSCWM years (1989, 1995).

years) were − 187 W/m² and − 178 W/m², respectively, while those in the previous winters of 1989 and 1995 (the weak years) were − 124 W/m² and − 162 W/m², respectively (Table 6). The ocean lost more heat to the atmosphere in the previous winter of a strong YSCWM

year and thus led to a cooler YSCWM in summer.

The five components of the air-sea heat flux used in the model were shortwave radiation, longwave radiation, sensible heat flux, latent heat flux and the adjustment term (Table 6). It was found that the ocean did

**Fig. 8.** Time series of the average water temperature (a, b) and temperature anomalies (c, d) at the sea surface and at a depth of 50 m in the Yellow Sea in the five YSCWM representative years.
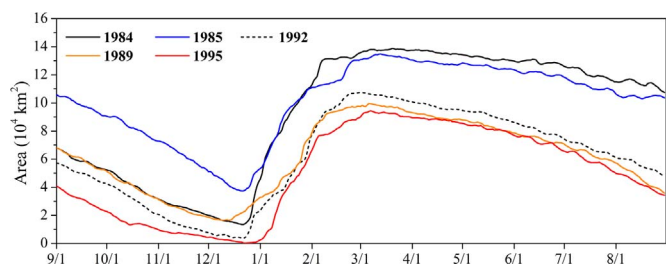


**Fig. 9.** Time series of the simulated cold water area with temperatures less than 8 °C at a depth of 50 m in the five YSCWM representative years.
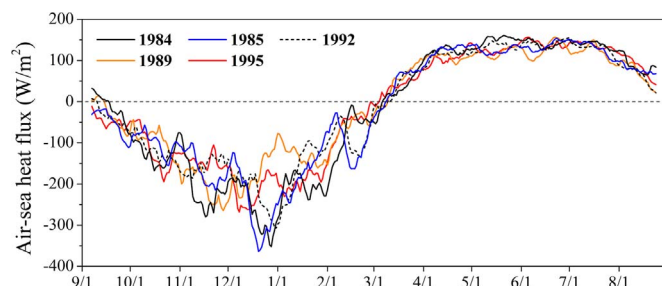


**Fig. 10.** Air-sea heat flux over the Yellow Sea in the five YSCWM representative years.

**Table 4**
Forcing conditions for the sensitivity experiments (based on the simulation of 1995).

| Experiment | Forcing conditions |
| --- | --- |
| INITIAL | Water conditions in September of 1983 |
| HEAT | Air-sea heat flux from September in 1983 to September in 1984 |
| WIND | Wind from September in 1983 to September in 1984 |
| EVA | Evaporation from September in 1983 to September in 1984 |
| PRE | Precipitation from September in 1983 to September in 1984 |
| SLP | Sea level pressure from September in 1983 to September in 1984 |
| Autumn-HEAT | Air-sea heat flux from September in 1983 to November in 1983 |
| Winter-HEAT | Air-sea heat flux from December in 1983 to February in 1984 |
| Spring-HEAT | Air-sea heat flux from March in 1984 to May in 1984 |
| Summer-HEAT | Air-sea heat flux from June in 1984 to August in 1984 |

**Table 5**
The contribution rate (α) of forcings to the differences of the average water temperature and area of the YSCWM between the strong (1984) and weak (1995) YSCWM years.

| Experiment | Temperature | | Area | |
| --- | --- | --- | --- | --- |
| | The 50 m depth | The 36°N section | The 50 m depth | The 36°N section |
| INITIAL | 11% | 9% | 26% | 40% |
| HEAT | 80% | 49% | 74% | 91% |
| WIND | − 6% | − 5% | − 13% | − 26% |
| EVA | 2% | 4% | 3% | − 1% |
| PRE | 2% | 6% | 1% | − 1% |
| SLP | 0.1% | − 1% | − 0.1% | − 2% |
| Autumn-HEAT | 3.2% | 2.7% | 7.5% | 7.1% |
| Winter-HEAT | 64% | 40% | 58% | 76% |
| Spring-HEAT | 18% | 13% | 32% | 28% |
| Summer-HEAT | 0.5% | − 0.4% | 0.2% | 2.1% |

not necessarily gain less solar radiation in the previous winter of the strong YSCWM years (1984 and 1985). The sea surface obtained 135 W/m² and 121 W/m² of heat in the strong YSCWM year of 1984 and 1985, respectively, which were larger than that in the weak YSCWM year of 1989 (111 W/m²). However, the ocean was characterized by losing more heat in the previous winter of the strong YSCWM years than weak YSCWM years. Among these components, the sensible heat was the key factor. Using a strong year (1984) and weak year (1995) as examples, the differences of the sensible heat contributed 66% of the total difference of air-sea heat flux between the previous winter of 1984 and 1995. This could be attributed to that the air-sea temperature difference in strong years (6.90 °C in 1984, 6.96 °C in 1985) was larger than these in weak years (5.34 °C in 1989, 6.18 °C in 1995), and the wind speed was also larger in strong years (6.70 m/s in 1984, 6.82 m/s in 1985) than weak years (6.58 m/s in 1989, 6.61 m/s in 1995) (Table 6) (Friehe and Schmitt, 1976).

## 4. Discussion

### 4.1. Relationship between the YSCWM and air-sea heat flux in the previous winter

As demonstrated in Section 3, the air-sea heat flux in the previous winter was a key factor that controlled the YSCWM intensity in strong and weak YSCWM years. In order to verify whether the air-sea heat flux in the previous winter was dominant factor to the YSCWM intensity over an interannual scale, rather than just occasionally for the two years (1984 and 1995), a set of numerical experiments was performed from 1981 to 1998 when the daily air-sea heat flux was available online. In these experiments, we used the air-sea heat fluxes in previous winter (from previous December to this February) in a specific year from 1981 to 1998 to replace the corresponding ones in the simulation of 1992. The initial conditions, the other air-sea conditions (such as

**Table 6**

The variables related to the air-sea heat flux (W/m²) in the previous winter of the strong and weak years of the YSCWM.

| Variables from the previous December to this February | 1984 | 1985 | 1989 | 1995 |
|---|---|---|---|---|
| Air-sea heat flux (W/m²) | − 187 | − 178 | − 124 | − 162 |
| Shortwave (W/m²) | 115 | 108 | 103 | 113 |
| Long wave (W/m²) | − 97.9 | − 85.8 | − 77.9 | − 93.4 |
| Sensible heat (W/m²) | − 99.2 | − 96.3 | − 61.8 | − 82.7 |
| Latent heat (W/m²) | − 125 | − 117 | − 95.2 | − 128 |
| Adjustment (W/m²) | 20.1 | 13.1 | 7.90 | 29.1 |
| Air-sea temperature difference (°C) | 6.90 | 6.96 | 5.34 | 6.18 |
| Wind speed ( m/s ) | 6.70 | 6.82 | 6.58 | 6.61 |

Note: The air-sea heat flux is positive when the sea obtains heat.

wind stress, surface level pressure, precipitation, and evaporation rates), and the open boundary conditions were kept the same as those in the simulation of 1992. The modelled interannual variations of the YSCWM were compared to the observations.

$T_{50w}$ and $S_{50w}$ were used to represent the modelled average water temperature and the YSCWM area at a depth of 50 m in the western part of the south YS (orange rectangle in Fig. 2) where observations were available; $T_{50}$ and $S_{50}$ were used to represent those for the entire YSCWM at a depth of 50 m. The correlation coefficient was 0.64 for the simulated and observed temperatures in the western YSCWM (Fig. 11a) and was 0.73 for the simulated and observed area of the YSCWM in the western YSCWM (Fig. 11b), both of which has a significant level over 99%. The significant positive correlations indicated that the interannual variations of the YSCWM can be reproduced by changing the air-sea heat flux in the previous winter because other boundary conditions for the simulations over those years were the same as those of the normal year of 1992. In addition, $T_{50}$ and $S_{50}$ were apparently related to $T_{50w}$ and $S_{50w}$ with correlation coefficients of 0.99 and 0.97, respectively (Fig. 11), suggesting that the interannual variations of the entire



**Fig. 11.** Time series of the average water temperature ($T_{50w}$, $T_{50}$) (a) and area ($S_{50w}$, $S_{50}$) (b) of the YSCWM in August at 50 m depth from 1981 to 1998. $T_{50w}$ and $S_{50w}$ are those for western part of YSCWM, $T_{50}$ and $S_{50}$ are those for entire YSCWM.

YSCWM intensity were consistent with those in the western part of the south YS.

In addition, the observed and modelled YSCWM intensities in this study were consistent with those from previous studies. Park et al. (2011) suggested the existence of three cold periods (1967–1971, 1983–1988 and 1996–2000) and two warm periods (1972–1980 and 1990–1995) for the YSCWM based on analyses of observed temperatures offshore from the Korea Peninsula from 1967 to 2008. Zhang and Yang (1996) reported that 1984 was the strongest year for the northern YSCWM, according to the observation data along a section between Dalian and Chengshan Jiao (green solid line in Fig. 1) of 42 years among 1928–1990.

### 4.2. Implication to prediction of the YSCWM intensity

Based on the analysis above, we found that the interannual variation of the YSCWM intensity in summer was mainly controlled by air-sea heat flux in the previous winter. This encouraged us to infer the YSCWM intensity by establishing a simple equation using air-sea heat flux in the previous winter. This way should be helpful to people who want to roughly predict the YSCWM intensity for the following summer but do not want to run a three-dimensional prediction model.

According to the results of the numerical experiments in Section 3.4, the air-sea heat flux in the previous winter was the principal factor that influenced the interannual variation of the YSCWM intensity. When establishing the regression equation, the satellite-derived average net sea surface heat flux (the sum of the shortwave radiation, longwave radiation, sensible heat flux, latent heat flux denoted by $HF_{winter}$, W/m²) and the mean sea surface temperature (denoted by $SST_{winter}$, °C) from NCEP over the YS in the previous cooling season (from the previous December to this February) were taken into consideration. Since the initial water condition in the previous autumn was also expected to affect the YSCWM intensity, the mean sea surface temperature ($SST_{init}$, °C) over the YS before the cooling season (i.e., on December 1) was also included in the regression equation.

Using all the available observational data for 1978–1998, following linear relationship between the YSCWM intensity, represented by the average water temperature in the western YSCWM ($T_{50w}$) and $SST_{init}$, $HF_{winter}$, $SST_{winter}$ was obtained.

$$T_{50w} = 1.2 \times 10^{-2} \cdot SST_{init} + \left( 9.30 \times 10^{-2} \cdot \frac{HF_{winter} \times S \times T}{C_p \times S \times d \times \rho} + 2.06 \right.$$
$$\left. \times 10^{-1} \cdot SST_{winter} \right) + 6.13 \tag{5}$$

Where $S$ is the area of the entire YS ($3.8 \times 10^{11}$ m²), $T$ is the cooling time in the previous winter (79488000 s), $C_p$ is the specific heat capacity of seawater (4096 J·kg⁻¹·°C⁻¹), $d$ is the average water deep of the YS (44 m), $\rho$ is the seawater density (1025 kg·m⁻³). After unifying the unit of each term in Eq. (5) to degree for temperature, we obtained following formula:

$$T_{50w} = 1.2 \times 10^{-2} \cdot SST_{init} + (4.00 \times 10^{-3} \cdot HF_{winter} + 2.06 \times 10^{-1} \cdot SST_{winter})$$
$$+ 6.13 \tag{6}$$

The items in the bracket within Eq. (6) represent the effect of the air-sea heat flux during the cooling season that was decided by the downloaded heat flux and the modulation of SST as given in Eq. (3). The physical meaning of prediction equation was that the YSCWM intensity in summer depended slightly on the water temperature before the cooling ($SST_{init}$), strongly on the cooling process during the previous winter ($HF_{winter}$, $SST_{winter}$, Fig. 8 and Fig. 9). Therefore, a good prediction means that the water property at the end of winter is well preserved in next summer.

The time series of $T_{50w}$ from 1981 to 1998 (circles in Fig. 12) calculated using Eq. (6) were compared with $T_{50w}$ observed (dots in
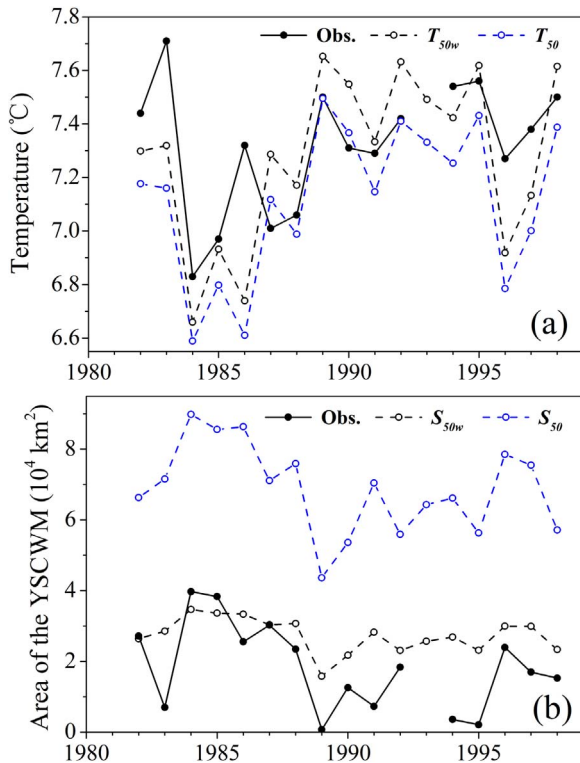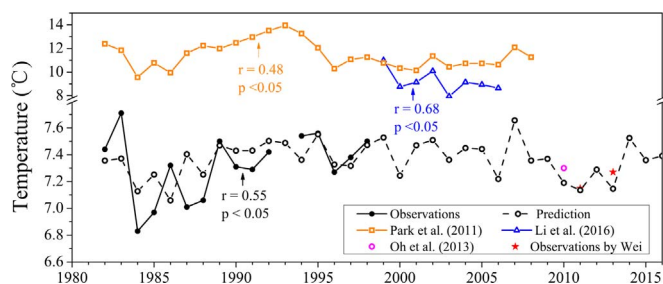
**Fig. 12.** Reconstructed YSCWM average water temperature ($T_{50w}$) and some observed water temperatures. The blue triangles mark the average water temperature below 30 m along the 36°N section in the western part of the Yellow Sea (Li et al., 2016). The orange squares highlight the spatially averaged temperature at a depth of 50 m (33–37°N, 124.4–126°E) in the eastern part of the Yellow Sea using the Korea Oceanographic Data Center (KODC) dataset (Park et al., 2011). (For interpretation of the references to color in this figure legend, the reader is referred to the web version of this article.)

Fig. 12). The correlation coefficient was 0.55, with a significant level of 95%. It was found that the prediction was not applicable in 1986 and 1987 compared with observation (Fig. 12). When removing the two years, the correlation coefficient raised to 0.76 with a significant level of 99%. Therefore, not only heat flux but also some other factors likely influenced the YSCWM intensity in 1986 and 1987. The horizontal lateral transport of heat, the phase of PDO and western Pacific Kuroshio heat transfer (Wei et al., 2013; Shi et al., 2014) are possible candidates.

Using this simple formula, we reconstructed the time series of $T_{50w}$ from 1999 to 2016 (circles in Fig. 12). Since no observational data for this period were available, we collected relevant observational data from the literature to validate Eq. (6). Li et al. (2016a) calculated the average water temperature below 30 m along the 36°N section in the western area of the YS from 1999 to 2006 (triangles in Fig. 12). Although these values were generally higher than $T_{50w}$ given by Eq. (6), the two time series showed a consistent variation with a correlation coefficient of 0.68. Park et al. (2011) reported the spatially averaged temperature at a depth of 50 m in the eastern part of the YS (33–37°N, 124.4–126°E) from 1981 to 2008 using data from the KODC (squares in Fig. 12). The correlation coefficient between the data given by Park et al. (2011) and those determined from Eq. (6) was 0.48, with a significant level of 95%. Some episodic observations of temperatures at a depth of 50 m inside the eastern YSCWM in August of 2010 (Oh et al., 2013) and those in the calculating area (Fig. 2a) in August of 2011 and 2013 (unpublished data provided by Prof. Wei Hao from Tianjin University of China) also conformed to the estimations from Eq. (6) (Fig. 12). The agreement between the observations and calculations from Eq. (6) also indicated the crucial role of the air-sea heat flux on the YSCWM intensity. Only using the data available online (for example, the NCEP/NCAR reanalysis data, the European Center for Medium-Range Weather Forecasts), instead of running the complicated numerical model, we can roughly predict the YSCWM intensity for the following summer.

## 5. Conclusion

The in-situ data from 1978 to 1998 show significant interannual variations of the YSCWM in August that occurred consistently in the horizontal and vertical directions. Specifically, the YSCWM is strong in 1984 and 1985, normal in 1992, and weak in 1989 and 1995. There are negative correlations between the average water temperatures and areas of the YSCWM in summer.

A three-dimensional hydrodynamic model is used to simulate the formation process of the YSCWM in the five specific years (1984, 1985, 1989, 1992, and 1995). The results suggest that the cooling process from the previous December to this February plays a crucial role in determination of the YSCWM intensity during summer. Specifically, the air-sea heat flux in the previous winter contributes ~60% to the water

temperature difference in August between the strong and weak YSCWM years. Among components of heat fluxes, sensible heat is the main contributor to the difference in the previous winter between strong and weak YSCWM years.

Following above results, the YSCWM intensity in summer is reconstructed using sea surface temperature in the previous early December and the air-sea heat flux in the previous winter over the entire YS. The interannual variations of reconstructed YSCWM intensity show a good correlation with the observed one. In the future, not only local factors but also remote factors should be considered in the reconstructing of YSCWM intensity in summer.

## References

Azumaya, T., Ohtani, K., 1995. Effect of winter meteorological conditions on the formation of the cold bottom water in the eastern Bering Sea shelf. J. Oceanogr. 51 (6), 665–680.

Blumberg, A.F., Mellor, G.L., 1987. A description of a three-dimensional coastal ocean circulation model. Three-Dimens. Coast. Ocean Models 1–16.

Brown, J., Hill, A.E., Fernand, L., Horsburgh, K.J., 1999. Observations of a seasonal jet-like circulation at the central North Sea cold pool margin. Estuar. Coast. Shelf Sci. 48 (3), 343–355.

Chen, D.X., Sun, X.P., Pu, Y.X., 1992. Marine Atlas of Bohai Sea, Yellow Sea, East China Sea. Hydrology.

Cho, K.D., 1982. On the influence of the yellow Sea bottom cold water on the demersal fishing grounds. Bull. Korean Fish. Technol. Soc. 18 (1), 25–33.

Dickey-Collas, M., Brown, J., Fernand, L., Hill, A.E., Horsburgh, K.J., Garvine, R.W., 1997. Does the western Irish Sea gyre influence the distribution of pelagic juvenile fish? J. Fish. Biol. 51 (sA), 206–229.

Du, B., 1996. The characteristics of cold water mass variation at the bottom of the North Yellow Sea and its hydrological effects on the mortality of shellfish cultured in the waters of outer Changshun Islands. Mar. Sci. Bull.Tianjin 15, 17–28 (in Chinese).

Ezer, T., Mellor, G.L., 1992. A numerical study of the variability and the separation of the Gulf Stream, induced by surface atmospheric forcing and lateral boundary flows. J. Phys. Oceanogr. 22 (6), 660–682.

Friehe, C., Schmitt, K., 1976. Parameterization of air-sea interface fluxes of sensible heat and moisture by the bulk aerodynamic formulas. J. Phys. Oceanogr. 6 (6), 801–809.

Grebmeier, J.M., Overland, J.E., Moore, S.E., Farley, E.V., Carmack, E.C., Cooper, L.W., Frey, K.E., Helle, J.H., McLaughlin, F.A., McNutt, S.L., 2006. A major ecosystem shift in the northern Bering Sea. Science 311 (5766), 1461–1464.

Guan, B.X., 1963. A preliminary study of the variation of the temeprature and the characteristics of the circulation of the Yellow Sea Cold Water Mass. Oceanol. Et. Limnol. Sin. 5 (4), 255–284 (in Chinese).

Guo, X.Y., Hukuda, H., Miyazawa, Y., Yamagata, T., 2003. A triply nested ocean model for simulating the Kuroshio-Roles of horizontal resolution on JEBAR. J. Phys. Oceanogr. 33 (1), 146–169.

He, C.B., Wang, Y.X., Lei, Z.Y., Xu, S., 1959. The formation of the Yellow Sea Cold Water and an elementary discussion of its properties. Oceanol. Et. Limnol. Sin. 2, 11–15 (in Chinese).

Hill, A.E., 1996. Spin-down and the dynamics of dense pool gyres in shallow seas. J. Mar. Res. 54 (3), 471–486.

Hill, A.E., Durazo, R., Smeed, D.A., 1994. Observations of a cyclonic gyre in the western Irish Sea. Cont. Shelf Res. 14 (5), 479–490.

Horsburgh, K.J., Hill, A.E., Brown, J., Fernand, L., Garvine, R.W., Angelico, M.M.P., 2000. Seasonal evolution of the cold pool gyre in the western Irish Sea. Progress. Oceanogr. 46 (1), 1–58.

Houghton, R.W., Schlitz, R., Beardsley, R.C., Butman, B., Chamberlin, J.L., 1982. The Middle Atlantic Bight cold pool: evolution of the temperature structure during

summer 1979. J. Phys. Oceanogr. 12 (10), 1019–1029.

Hur, H.B., Jacobs, G.A., Teague, W.J., 1999. Monthly variations of water masses in the Yellow and East China Seas, November 6, 1998. J. Oceanogr. 55 (2), 171–184.

Jiang, B.J., Bao, X.W., Wu, D.X., Xu, J.P., 2007. Interannual variation of temperature and salinity of northern Huanghai Sea Cold Water Mass and its probable cause. Acta Oceanol. Sin. 29 (4), 1–10 (in Chinese).

Johnson, D.R., Teague, W.J., 2002. Observations of the Korea Strait bottom cold water. Cont. Shelf Res. 22 (5), 821–831.

Kim, Y.H., Kim, Y.B., Kim, K., Chang, K., Lyu, S.J., Cho, Y.-K., Teague, W.J., 2006. Seasonal variation of the Korea Strait cold water and its relation to the bottom current. Geophys. Res. Lett. 33 (24).

Li, A., Yu, F., Si, G., Wei, C., 2016a. Long-term temperature variation of the Southern Yellow Sea Cold Water Mass from 1976 to 2006. Chin. J. Oceanol. Limnol. 1–13.

Li, H., Xiao, T., Ding, T., Lü, R., 2006. Effect of the Yellow Sea Cold Water Mass (YSCWM) on distribution of bacterioplankton. Acta Ecol. Sin. 26 (4), 1012–1019.

Li, J., Li, G., Xu, J., Dong, P., Qiao, L., Liu, S., Sun, P., Fan, Z., 2016b. Seasonal evolution of the Yellow Sea Cold Water Mass and its interactions with ambient hydrodynamic system. J. Geophys. Res.: Oceans 121 (9), 6779–6792.

Li, K.P., 1991. Responses of the Yellow Sea Cold Water Mass to ocean variation. Acta Oceanol. Sin. 13 (6), 779–785 (in Chinese).

Li, X., Wang, X., Chu, P.C., Zhao, D., 2015. Low-frequency variability of the Yellow Sea Cold Water Mass identified from the China coastal waters and adjacent seas re-analysis. Adv. Meteorol.

Lie, H.J., Cho, C.H., Lee, J.H., Lee, S., 2001. Does the Yellow Sea warm current really exist as a persistent mean flow? J. Geophys. Res.: Oceans 106 (C10), 22199–22210.

Liu, X., Huang, B., Huang, Q., Wang, L., Ni, X., Tang, Q., Sun, S., Wei, H., Liu, S., Li, C., Sun, J., 2015. Seasonal phytoplankton response to physical processes in the southern Yellow Sea. J. Sea Res. 95, 45–55.

Luyten, P.J., Jones, J.E., Proctor, R., 2003. A numerical study of the long-and short-term temperature variability and thermal circulation in the North Sea. J. Phys. Oceanogr. 33 (1), 37–56.

Mellor, G., 2003. The three-dimensional current and surface wave equations. J. Phys. Oceanogr. 33 (9), 1978–1989.

Na, H., Kim, K.Y., Chang, K.I., Kim, K., Yun, J.Y., Minobe, S., 2010. Interannual variability of the Korea Strait Bottom Cold Water and its relationship with the upper water temperatures and atmospheric forcing in the Sea of Japan (East Sea). J. Geophys. Res.: Oceans 115 (C9).

Oh, K.H., Lee, S., Song, K.M., Lie, H.J., Kim, Y.T., 2013. The temporal and spatial variability of the Yellow Sea Cold Water Mass in the southeastern YS, 2009–2011. Acta Oceanol. Sin. 32 (9), 1–10.

Park, S., Chu, P.C., Lee, J.H., 2011. Interannual-to-interdecadal variability of the Yellow Sea Cold Water Mass in 1967–2008: characteristics and seasonal forcings. J. Mar. Syst. 87 (3), 177–193.

Shi, Q., 2014. Climate response and spatial-temporal model of the inter-annual change of winter temperature-salinity in the South Yellow Sea. Mar. Sci. Bull. 33 (2), 148–156 (in Chinese).

Song, X., Lin, X., Wang, Y., 2009. The preliminary study of long-term variability of the Yellow Sea cold water in summer and its possible reasons. J. Guangdong Ocean Univ. 29 (3), 59–63 (in Chinese).

Stabeno, P.J., Bond, N.A., Salo, S.A., 2007. On the recent warming of the southeastern Bering Sea shelf. Deep Sea Res. Part II: Top. Stud. Oceanogr. 54 (23), 2599–2618.

Su, Y.S., Weng, X.C., 1994. Water masses in China seas. In: Oceanology of China Seas. Springer, Netherlands, pp. 3–16.

Wang, B., Hirose, N., Kang, B., Takayama, K., 2014a. Seasonal migration of the Yellow Sea Bottom Cold Water. J. Geophys. Res.: Oceans 119 (7), 4430–4443.

Wang, D., Huang, B., Liu, X., Liu, G., Wang, H., 2014b. Seasonal variations of phytoplankton phosphorus stress in the Yellow Sea Cold Water Mass. Acta Oceanol. Sin. 33 (10), 124–135.

Wang, Q., Guo, X., Takeoka, H., 2008. Seasonal variations of the Yellow River plume in the Bohai Sea: a model study. J. Geophys. Res.: Oceans 113 (C8).

Wang, R., Zuo, T., Wang, K.E., 2003. The Yellow Sea cold bottom water—an over-summering site for Calanus sinicus (Copepoda, Crustacea). J. Plankton Res. 25 (2), 169–183.

Warrach, K., 1998. Modelling the thermal stratification in the North Sea. J. Mar. Syst. 14 (1–2), 151–165.

Wei, H., Shi, J., Lu, Y., Yuan, P., 2010. Interannual and long-term hydrographic changes in the Yellow Sea during 1977–1998. Deep Sea Res. Part II: Top. Stud. Oceanogr. 57 (11), 1025–1034.

Wei, H., Yuan, C., Lu, Y., Zhang, Z., Luo, X., 2013. Forcing mechanisms of heat content variations in the Yellow Sea. J. Geophys. Res.: Oceans 118 (9), 4504–4513.

Weng, X., Zhang, Y., Wang, C., Zhang, Q., 1989. The variational characteristics of the Huanghai Sea (Yellow Sea) cold water mass. J. Ocean Univ. Qingdao. S1 (in Chinese).

Wyllie-Echeverria, T., Wooster, W.S., 1998. Year-to-year variations in Bering Sea ice cover and some consequences for fish distributions. Fish. Oceanogr. 7 (2), 159–170.

Xin, M., Ma, D., Wang, B., 2015. Chemicohydrographic characteristics of the Yellow Sea Cold Water Mass. Acta Oceanol. Sin. 34 (6), 5–11.

Yang, H.W., Cho, Y.K., Seo, G.H., You, S.H., Seo, J.W., 2014. Interannual variation of the southern limit in the Yellow Sea Bottom Cold Water and its causes. J. Mar. Syst. 139, 119–127.

Yu, X., Guo, X., Takeoka, H., 2016. Fortnightly Variation in the Bottom Thermal Front and Associated Circulation in a Semienclosed Sea. J. Phys. Oceanogr. 46 (1), 159–177.

Yuan, D., Li, Y., Qiao, F., Zhao, W., 2013. Temperature inversion in the Huanghai Sea bottom cold water in summer. Acta Oceanol. Sin. 32 (3), 42–47.

Zhang, S.W., Wang, Q.Y., Lü, Y., Cui, H., Yuan, Y.L., 2008. Observation of the seasonal evolution of the Yellow Sea Cold Water Mass in 1996–1998. Cont. Shelf Res. 28 (3), 442–457.

Zhang, Y.K., He, X.M., 1981. The annual variation and its fore-casting of the intensity of cold water mass of the western-north Yellow Sea in spring. Period. Ocean Univ. China 19 (s1), 275–283 (in Chinese).

Zhang, Y.K., Yang, Y.L., 1996. Analyses of the variational characteristics of the north Huang Hai Sea Cold Water Mass. Mar. Forecasts 13 (4), 15–21 (in Chinese).